

Determining Hydraulic Permeability Distributions in Cancellous Bone

Jinsoo Uh, A. Ted Watson*

Department of Chemical & Biological Engineering, Colorado State University, Fort Collins, CO 80523-1370, USA

*ted.watson@colostate.edu

Abstract- Hydraulic permeability of cancellous bone is an important property for modeling bone and fluid response to mechanical stimuli. It can play a role in design of bone substitutes and cementation procedures. However, this property is poorly understood. Published experimental studies have reported large variations in property values, and there remains no reliable method for predicting the permeability from other observations or measurements.

Consideration of spatial variations in properties within laboratory samples raises significant issues regarding the efficacy of permeability determinations from conventional experiments. We use magnetic resonance imaging (MRI) to probe fluid flow and fluid residence at a much finer scale than can be assessed with conventional experiments. We use this information to resolve spatial distributions of porosity and permeability on a bone sample.

Keywords- Hydraulic Permeability; Cancellous Bone; Magnetic Resonance Imaging; Spatially Distributed Properties.

I. INTRODUCTION

The hydraulic permeability is one of several sample-specific properties that can be used within poroelastic theory to simulate bone and fluid response to mechanical stimuli [1, 2]. The hydraulic permeability can be valuable for the design and conduct of cementation procedures for joint replacement, prosthesis attachment, and bone cement augmentation [3, 4]. Permeability has been identified as a key explanatory variable for vascularization of bone implants [5], and is an important consideration in the design of artificial bone substitutes [6].

It would be highly desirable to predict permeability from more conveniently determined characteristics, such as geometrical indices (e.g., bone fraction and specific area [7, 8]), perhaps together with other measurements such as nuclear magnetic resonance [9, 10]. Such relationships could aid investigations of artificial bone substitutes and could possibly enable determination of patient-specific permeability properties *in vivo*. However, no reliable prediction methods have yet emerged.

An important element for such investigations is a reliable means to determine properties from representative samples. While there have been several studies directed to determining the permeability of bone samples [3, 11, 12, 13, 14, 15], the relatively large range of reported values suggest this property is not well understood. It seems likely that experimental artifacts contribute to this dilemma [2, 16]. One significant issue not addressed previously is spatial variability of properties within laboratory samples.

Whereas only single values of permeability are calculated from conventional experiments, we know that this property can vary spatially within permeable media. Such spatial variations within samples could contribute to a poor resolution of permeability with conventional experiments. In particular, the characterization of anisotropic permeability from conventional experiments should be reconsidered, as even isotropic, but spatially variable, permeability will lead to different observations of permeability in different flowing directions. Such gross characterization of properties can significantly degrade our ability to develop reliable means for predicting permeability.

We have developed a novel method for determining spatial distributions of permeability within permeable media [17]. Considerations at this scale prompts new questions about the reliability of permeability values obtained from conventional experiments.

Our experiments are related to conventional experimentation in that fluid is flowed into the sample at a constant rate, and the pressure drop is determined. Beyond conventional experimentation, we use magnetic resonance imaging (MRI) experiments to spatially resolve the porosity and flow rates within the sample. The permeability distribution is determined through solution of an associated inverse problem.

We have reported the development and application of MRI methods and inverse problem methodology for determining the permeability elsewhere [17, 18, 19]. Our goal here is to introduce this methodology within the context of characterizing bone properties, and to demonstrate its use with a bone sample.

First, we provide some background for modeling the flow of fluids in permeable media in order to motivate determination of property distributions. We then review the conventional method for determining permeability in light of spatial variability of such properties. We explain our methodology to determine permeability distributions, and present results obtained on a bone sample.

II. HYDRAULIC PROPERTIES AND THE INVERSE PROBLEM

Volume-averaging [20, 21], as well as other homogenization methods, provides a rigorous means for developing mathematical models that describe flow within disordered permeable media, such as cancellous bone. Volume-averaging is an extension of the well-known continuum description used to describe fluid flow. The continuum approach enables meaningful descriptions of physical systems, without requiring explicit consideration of molecular behavior, by introducing various material properties, such as the viscosity and density. Similarly, the volume-averaging approach enables meaningful descriptions of permeable systems by introducing a number of macroscopic properties that represent the permeable media. This approach specifies the correct functional relationships among the properties and fluid states while eliminating the need to specify the exact geometry of the solid/fluid interfaces—information that is typically unavailable by any means. Still, the media properties represent macroscopic empiricisms that must be specified in order to mathematically simulate flow.

The porosity and permeability are fundamental material properties required to describe flow through permeable media. These properties arise in the volume-averaged mass and momentum balances for creeping flow of a single fluid phase [22]. The volume-averaged mass balance (continuity equation) is:

$$\frac{\partial(\phi\rho)}{\partial t} = -\nabla \cdot (\rho \mathbf{v}) \quad (1)$$

where \mathbf{v} is the (volume-averaged) superficial velocity, ρ the fluid density, and ϕ the porosity. The volume-averaged momentum balance for creeping flow is Darcy's law:

$$\mathbf{v} = -\frac{\mathbf{K}}{\mu} \cdot (\nabla p - \rho \mathbf{g}) \quad (2)$$

where p is the (volume-averaged) pressure, μ the fluid viscosity, \mathbf{g} the acceleration of gravity, and \mathbf{K} the permeability. The media properties—porosity and permeability—are continuous functions of position. The permeability is a second-order tensor, although in many cases it is taken to be isotropic. Additional balance equations and media properties may be required to describe more complex situations, such as consideration of elastic bone and fluid responses to external stress stimuli [1]. Nevertheless, the porosity and permeability, which are solely determined by the medium structure, and the previously stated fluid properties are sufficient here.

The porosity, which is related to the bone-volume-fraction by the equation $BVF = 1 - \phi$, is defined as the ratio of the void volume to the total volume. Any experimental method that can provide the means to determine the void volume corresponding to a given observation volume will provide the average property for that spatial region. On the other hand, the permeability is an *effective* property which is *defined* by eq. 2—i.e., at any position, it is the proportionality between the gradient of the locally-averaged pressure (divided by the fluid viscosity) and the locally-averaged superficial velocity. To determine the permeability, one must mathematically model an experiment and calculate the permeability from observations of the system states and properties. This is an *inverse problem*, in that you observe the dependent variables within the model equations in order to determine a property within those equations.

Consider now the conventional method to determine the permeability for a sample. Suppose we have a parallelepiped sample that is sealed around the periphery, except for the injection and production faces at either end of the sample (see Fig. 1). An incompressible fluid is injected at a constant flow rate through the sample, and the flow rate and pressure drop are determined. We now develop the associated inverse problem to determine the permeability.

For incompressible flow, the continuity equation reduces to

$$\nabla \cdot \mathbf{v} = 0. \quad (3)$$

The following conditions are specified around the periphery of the sample (see Fig. 1):

$$\begin{aligned} p(0, z_2, z_3) &= p_{in} - \rho g(z_3 - z_3^{in}) \\ p(L_1, z_2, z_3) &= p_{out} - \rho g(z_3 - z_3^{out}) \\ \mathbf{v}(z_1, z_2, z_3) \cdot \mathbf{n} &= 0, \quad \text{for } z_2 = 0, L_2 \\ \mathbf{v}(z_1, z_2, z_3) \cdot \mathbf{n} &= 0, \quad \text{for } z_3 = 0, L_3. \end{aligned} \quad (4)$$

z_3^{in} and z_3^{out} represent reference points at which p_{in} and p_{out} are specified, respectively. The unit vector \mathbf{n} is normal to the peripheral surfaces. Gravity is represented as a scalar in understanding that its direction is opposite to z_3 .

Assuming that the permeability is isotropic, the Darcy equation simplifies to:

$$v_{z_i} = -\frac{k}{\mu} \left(\frac{\partial p}{\partial z_i} \right), \quad i = 1, 2, 3. \quad (5)$$

If we further assume that the permeability is *spatially uniform*, conditions of no flow in the z_2 and z_3 directions are consistent with the continuity equation (eq. 3) and end conditions (eq. 4). Then, we integrate eq. 5 over the length L_1 and solve for the permeability:

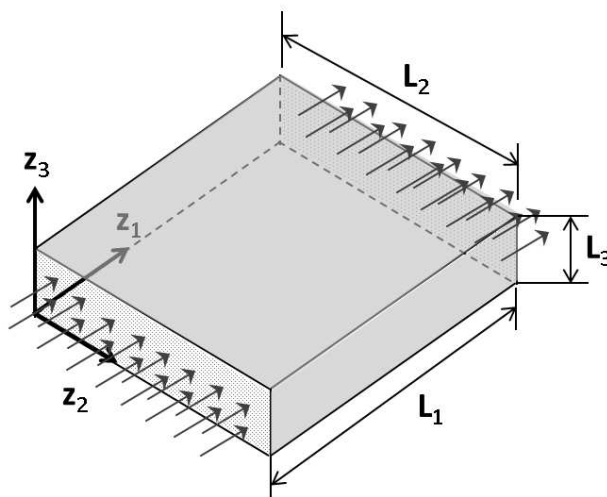


Fig. 1 The experimental sample domain. The lengths of the sample in z_1 , z_2 , and z_3 directions are L_1 , L_2 , and L_3 , respectively. The parallel arrows drawn on the injection and production faces indicate fluid flowing into and out of the domain along the z_1 direction. The gray-colored peripheral surfaces are boundaries across which fluid does not flow.

$$k^{app} = \mu \frac{Q}{A_c} \frac{L_1}{|\Delta p|}. \tag{6}$$

Q is the volumetric flow rate, A_c is the cross-sectional area of the sample, Δp is the pressure drop over the sample length L_1 , and k^{app} is the apparent permeability. We have used the term ‘apparent’ since the calculated value represents an artifact of the experiment. It is an intrinsic property value only if all the assumptions of the analysis are met.

Note that the experiment provides no evidence regarding the presence, or lack of, spatial variability in the permeability. That is, you can calculate a permeability value regardless of whether the permeability is uniform or not. Furthermore, should the permeability vary spatially, there is no evidence that the apparent value represents a meaningful average. Moreover, while some authors have sought to determine anisotropic permeabilities by performing conventional experiments and analyses in two, or three, orthogonal directions, these apparent permeability values will only be correct if the permeability is spatially uniform and the principle directions of anisotropy coincide with the experimental flow directions. Note that samples with spatially-variable isotropic permeability distributions will, in fact, exhibit different apparent permeabilities in different flow directions.

III. DETERMINING SPATIAL DISTRIBUTIONS OF PERMEABILITY

Our ultimate goal is to resolve the entire spatially-dependent permeability function, $\mathbf{K}(\mathbf{z})$, from experimental data. Although our mathematical formulation and experimental methodologies enable us to resolve three-dimensional, anisotropic spatial distributions of permeability, we pursue a less ambitious proof-of-principle here. Specifically, we assume the permeability is isotropic, although spatially variable. Furthermore, we have prepared our sample to be sufficiently thin in one direction (i.e., z_3) so that a two-dimensional mathematical model is sufficient.

The use of a thin length in one direction is a mathematical convenience that enables us to clearly illustrate the evidence of spatial variations in the properties. In general, the size of the sample is limited by the availability of representative material and the characteristics of the associated imaging equipment. Our system can accommodate one-inch cubic samples, which is a common size used in conventional bone permeability experiments. We have demonstrated our methodology with the associated three-dimensional mathematical analysis on a geological sample [17].

We use two different MRI experiments. Prior to initiating flow, spin-density imaging experiments are used with the fluid-saturated sample to determine the amount of fluid corresponding to each voxel in the sample [18]. This enables us to determine the spatial distribution of porosity. Then, while the sample is subject to fluid injection at a constant rate, velocity imaging experiments are conducted [23]. The porosity distribution is required to determine the spatially-resolved superficial velocity distribution from the measured velocities [17]. Finally, we solve an associated inverse problem in order to determine the permeability distribution [17].

Here, we demonstrate these steps using experimental results for a specific sample. An equine femur was harvested from a euthanized female horse. A rectangular piece of trabecular bone having a length of 23 mm in each of two spatial directions and thickness 5.0 mm was excised from the distal epiphysis. The sample was sonicated in trichloroethylene and flushed with high pressure water to remove blood, marrow, and bone fluid. The bone sample was placed between two rectangular parallelepiped

acrylic plates. The sample holder was made by a shrinking plastic film tube that covers the sample and the acrylic plates with two male connectors attached at both ends (Fig. 2). Porous membranes were placed between the sample and the flow entrance and exit to ensure parallel flow at the open edges of the sample. The sample and holder were vacuum saturated with water.

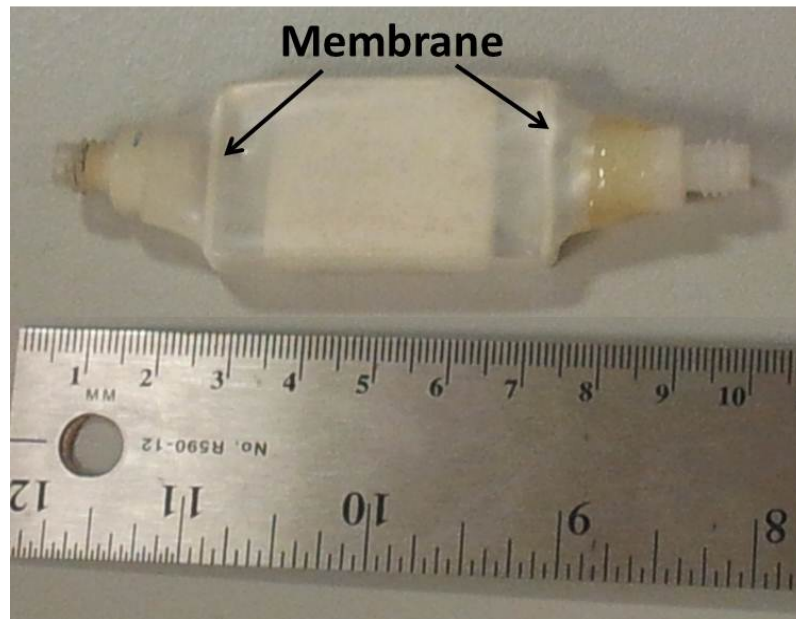


Fig. 2 The sample holder mounting a piece of trabecular bone for MR velocity imaging.

The MRI experiments were performed with a Bruker BioSpec[®] 24/30 system operating at 100 MHz and equipped with a 3.5-cm-diameter birdcage coil. Hydrogen nuclei within the saturating water are observed. Since all of our MRI experiments are conducted during static conditions or steady flow, the imaging times are not significant issues.

A. Porosity Distributions

Spatially resolved Carr-Purcell-Meiboom-Gill (CPMG) images were conducted and analyzed to determine accurate estimates of the amount of water within each voxel [18]. The average porosity for each voxel was then calculated. The voxel size is $0.78 \times 0.78 \times 5.0 \text{ mm}^3$. The spatial distribution of the porosity is shown in Fig. 3. This figure indicates that the bottom portion of the sample is relatively denser (i.e., this region has smaller values of the porosity) than the upper portion. The number distribution is provided in Fig. 4. Porosity values range from approximately 0.4 to 0.8. The average value for the sample was determined to be 0.60.

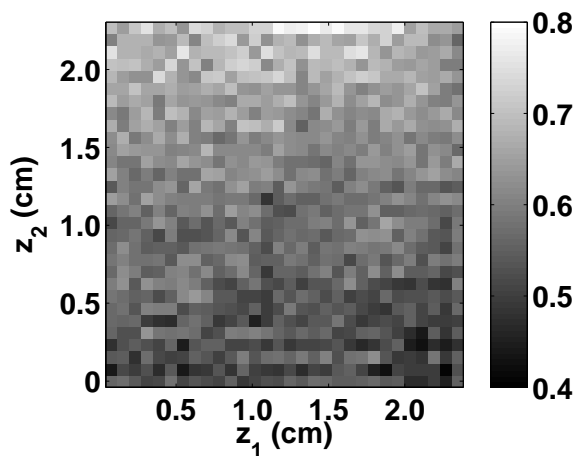


Fig. 3 Porosity distribution of the bone sample. The image shows porosity values at each of 30×30 voxels in the sample.

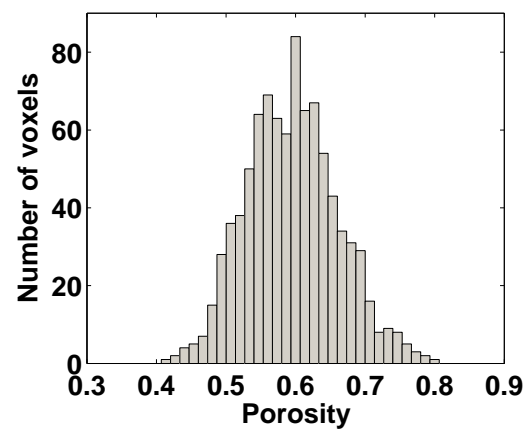


Fig. 4 Number distribution of porosity of the bone sample; the mean and standard deviation for the 30×30 voxels are 0.60 ± 0.07 .

B. Velocity Distributions

Two flow experiments were conducted on the sample. The overall direction of flow for Experiment A is in the direction of increasing values of z_1 , as represented by Fig. 1. The overall direction of Experiment B is in the direction of increasing values of z_2 (i.e., the axes z_1 and z_2 correspond to the physical sample). This was accomplished by disassembling the sample holder after Experiment A, rotating the sample 90 degrees, and remounting it in the holder for Experiment B.

A constant hydraulic head was maintained on the injection side, and the flow rate was measured. The apparent permeabilities calculated for Experiments A and B were 8.9 kD (kilo-Darcy) and 4.0 kD, respectively. Velocity imaging experiments were performed on each of the flow experiments. We used pulsed-field-gradient stimulated-echo (PFGSE) sequences. In order to accurately determine the velocities corresponding to each voxel, we used velocity encoding to determine the number distribution of the local velocity, and then computed the corresponding average velocities for each voxel [23]. The velocities were resolved in the two-dimensional domain by frequency encoding in the overall direction of flow and phase encoding in the other direction. The imaging parameters were: spatial field-of-view = $50 \times 25 \text{ mm}^2$, resolution = $0.78 \times 0.78 \text{ mm}^2$, repetition time = 5000 ms, echo time = 3.1 ms, observation time (separation of velocity encoding gradients) = 100 ms, velocity field-of-view = 5.0 mm/s, and velocity resolution = 0.16 mm/s.

The superficial velocities determined for each experiment are shown in Figs. 5a and 5b. The non-uniformity of the velocities clearly indicates that the permeability is not spatially uniform.

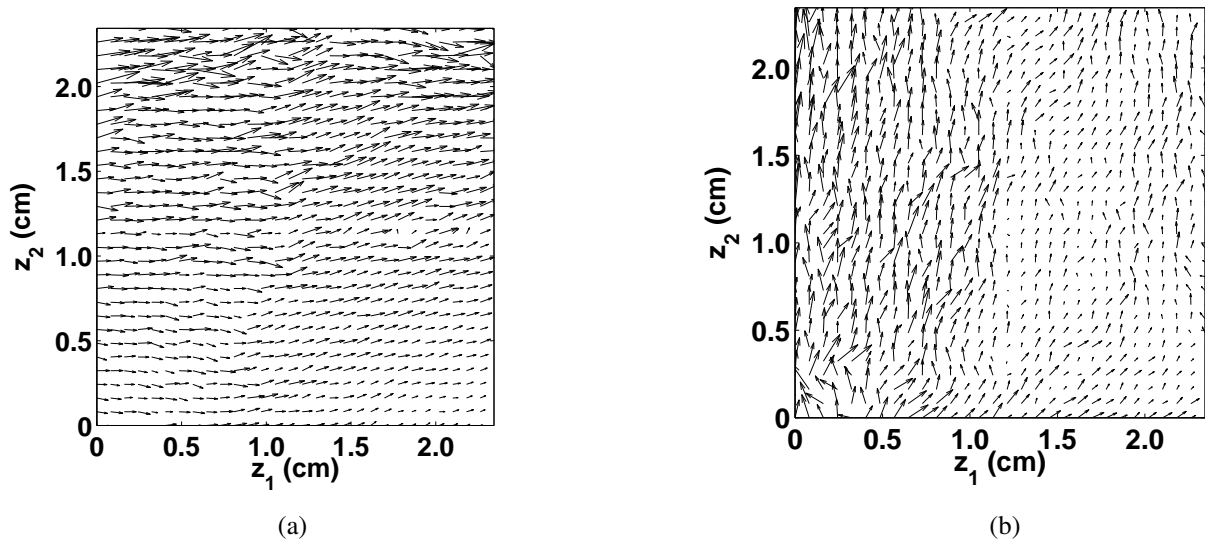


Fig. 5 Velocity images for Experiment A (a) and Experiment B (b). The velocity images correspond to each of the two (orthogonal) directions of flow across the sample. The size and angle of each arrow indicate the magnitude and direction of fluid flow for the corresponding voxel.

C. Permeability Distributions

The permeability distribution is determined from the velocity measurements by solution of an associated inverse problem. The mathematical model of the experiment is provided by Eqs. 2 and 3 with boundary conditions given by Eq. 4. The inverse problem corresponds to the determination of the permeability distribution $k(\mathbf{z})$ that minimizes the performance index:

$$\min_k J = J_{expt} + \lambda J_{reg} \tag{7}$$

The performance index consists of two terms. The first, J_{expt} , is a measure of the differences between the measured data and the corresponding values calculated using the mathematical model of the experiment with a given estimate of the permeability distribution. The regularization term, J_{reg} , serves to penalize undue variations in the estimated permeability function. This is desired since, ultimately, we are seeking to estimate a function on the basis of a finite (although relatively large) set of data.

Data from both experiments are used together to estimate the permeability. We expect that the two experiments will provide much more accurate estimates of the permeability distribution than either experiment alone. This approach will also avoid a possible lack of identifiability that could, in principle, arise from a single experiment [17, 19].

The first term, J_{expt} , is based on maximum-likelihood estimation [24]. Specifically, the corresponding terms for each experiment are summed:

$$J_{expt} = J_A + J_B. \tag{8}$$

For experiment I :

$$J_I = [\mathbf{Y}_I - \mathbf{F}_I]^T \mathbf{W}_I [\mathbf{Y}_I - \mathbf{F}_I], \quad (9)$$

where the vector \mathbf{Y}_I contains all the velocity measurements, \mathbf{F}_I contains the corresponding velocities calculated with a specified permeability distribution $k(\mathbf{z})$, and \mathbf{W}_I is a weighting matrix that is proportional to the inverse of the variance-covariance matrix of errors in the experimental measurements. In our work, we assume that the measurement errors have mean zero and are independent and identically distributed, so that the weighting matrix is the identity.

We use a standard form for the regularization term that promotes smoothness of the estimates by penalizing large values of the second derivative:

$$J_{reg} = \int_0^{L^2} \int_0^{L^1} \sum_{i=1}^2 \left(\frac{\partial^2 k(\mathbf{z})}{\partial z_i^2} \right)^2 dz_1 dz_2. \quad (10)$$

The regularization parameter λ is chosen by a heuristic method that considers the relative effects of the regularization and data-fitting terms [25]. In essence, our best estimate is the smoothest function that is consistent with the measured data.

We solve the model equations (Eqs. 2 and 3 with boundary conditions Eq. 4) by finite-differences [19]. We eliminate the velocity and solve for the pressure, and then use the Darcy equation (Eq. 2) to compute the velocities. We solve these equations on a grid that is finer than the resolution of data, and then compute the corresponding average value of velocities for each voxel to form the vector \mathbf{F} . A 64×64 finite-difference grid was used.

The permeability function is parameterized by tensor product B-splines, which are given by the product of univariate B-splines:

$$k(\mathbf{z}) = \sum_{i=1}^{N_1} \sum_{j=1}^{N_2} c_{i,j} B_i^m(z_1; \mathbf{x}_1) B_j^m(z_2; \mathbf{x}_2). \quad (11)$$

Here, m is the order of the B-spline, $B_i^m(z_j; \mathbf{x}_j)$ is the i th B-spline basis function on the extended partition \mathbf{x}_j (which contains locations of the knots in the z_j direction), and $c_{i,j}$ is a coefficient. B-splines are a superior way to represent unknown functions since they can approximate any continuous function on a finite domain arbitrarily accurately [26]. Thus, when sufficient numbers of knots are provided, we should be able to represent the *true*, but unknown, function by suitable selection of the coefficients $c_{i,j}$. We use order $m = 4$ and sufficient numbers of uniformly spaced knots so that the estimation problem is not affected by the partition. In this case, we used 34 knots in each direction. The regularization term is quadratic in the unknown parameters, assembled in the vector \mathbf{c} , and thus can be expressed as:

$$J_{reg} = \mathbf{c}^T \mathbf{H} \mathbf{c}. \quad (12)$$

The elements of the matrix \mathbf{H} are developed elsewhere [17].

The values of the coefficients \mathbf{c} that minimize Eq. 7 are determined using a quasi-Newton method that utilizes gradients of the performance index gradients that are determined by the method of adjoint states [19]. This is augmented with a global optimization method (parallel tempering) if termination at a local minimum is suspected [17].

The estimated permeability distribution is shown in Fig. 6. The value of permeability ranges over several orders of magnitude—from approximately 6 D to 60 kD. While a high degree of correlation between porosity and permeability is not necessarily expected, the sample texture indicated by the spatial distributions of porosity and permeability (Figs. 3 and 6(b), respectively) seems consistent. Namely, the denser (less porous) and less permeable region corresponds to the bottom of the sample, and in particular the right-hand region (i.e., large values for z_1). The less dense, and more permeable, region corresponds to the top of the sample.

The correlation between the velocity images and the permeability distribution is not so transparent. This is because the flow at any point is affected by the *entire* permeability distribution—not just the local permeability value. Nevertheless, the sample region corresponding to the lowest range of permeability values does have relatively small velocities in both experiments, and the region corresponding to the highest range of permeabilities has relatively large velocities in both experiments.

IV. DISCUSSION

The ability to probe local fluid storage and fluid flow at a relatively fine scale invites a reconsideration of flow experiments for the study of cancellous bone.

Irrespective of quantitative resolution of the properties, MRI can be used to investigate whether a sample might have anomalous features that invalidate its use for conventional experiments. Nevertheless, the determination of spatially resolved properties serves to mitigate that issue.

As noted in the introduction, one role of permeability experiments is to develop data bases that could be used to develop relationships among permeability and various other properties that may be more conveniently measured, or possibly available from *in vivo* measurements. Such relationships generally involve the determination of empirical or semi-empirical correlations among the considered parameters. Correlations developed on the basis of properties corresponding to identical spatial locations,

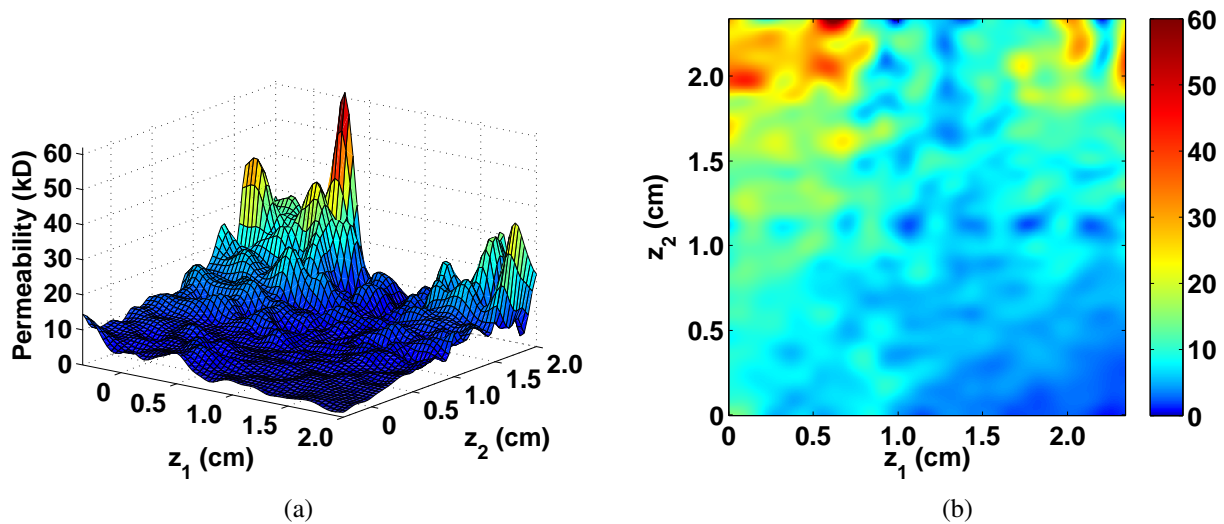


Fig. 6 Estimated permeability distribution for trabecular bone presented in three-dimensional plot (a) and two-dimensional image (b). The permeability exhibits a spatial variability ranging from 6.1 Darcy to 62 kilo-Darcy.

as opposed to the use of single-valued properties that represent only spatially-averaged or apparent values for entire laboratory samples, should provide for a more precise relationship. Furthermore, the spatially resolved properties provide for considerably larger data bases, which is an important consideration in developing correlations.

Our approach provides methodology to determine anisotropic permeability. Conventional methods provide only apparent permeabilities in selected flowing directions, which does not actually resolve anisotropic permeability.

The determination of anisotropic permeability distributions requires the specification of the symmetric, second order tensor $\mathbf{K}(\mathbf{z})$. While in principle one could set out to estimate the six independent functions (of position) associated with that tensor, this would seem to involve unnecessary degrees of freedom. It seems reasonable to assume that the directional aspect of the permeability anisotropy (which depends, in a sense, on the ‘texture’ or ‘fabric’) would vary much more slowly (with position) than does the magnitude. We propose that the permeability be represented as the product of a constant, symmetric matrix and a spatially dependent function:

$$\mathbf{K}(\mathbf{z}) = \mathbf{G}k_s(\mathbf{z}). \quad (13)$$

The components of \mathbf{G} could be estimated together with the parameters of the function $k_s(\mathbf{z})$. This could be effectively executed by sequentially, and interactively, estimating \mathbf{G} and $k_s(\mathbf{z})$ through solution of inverse problems similar to that used here.

To ensure reliable determination of the anisotropic permeability, one should reconsider the experimental design, as we have done for the spatially variable, isotropic situation [17, 19]. For example, are the data sufficient to resolve spatially-variable anisotropic permeability? This can be addressed by evaluating whether the data are consistent with a simplified representation, such as an isotropic representation, or one that is anisotropic, but spatially uniform. This requires the solution of those corresponding inverse problems, and evaluations of residuals, or other measures of the quality of fit.

Should additional information about the unknown properties be desired, there are some modifications in experimental design that can be pursued. Measurements of pressures at locations along the sample surface can provide additional information to determine the unknown properties [19]. One can also use additional experiments in which portions of the entrance and exit surfaces are blocked so that the flow within the sample is modified [17].

Application to cortical bone provides some additional challenges. In principle, the Darcy equation, with spatially-dependent permeability and porosity, can be used to model cortical bone. However, MRI experiments are more challenging with cortical bone. The relatively small amount of saturating fluid results in a relatively small signal, and the transverse relaxation can be relatively fast. We do not know the degree to which porosity and permeability distributions in cortical bone can be resolved with our methodology. Nevertheless, there are MRI experiments that can provide important information about structure and properties of cortical bone, even if those properties are not resolved in the same way as was done in this study.

V. CONCLUSIONS

Magnetic resonance imaging provides the means to probe spatial distributions of fluid storage and flow within permeable samples. We have demonstrated the use of MRI measurements to determine porosity and velocity distributions within cancellous bone. This information was in turn used to determine the permeability distribution. The results show significant spatial variations

of these properties throughout the sample. Such spatial variability has important implications for the efficacy of conventional permeability experiments.

ACKNOWLEDGEMENTS

We thank U.S. Department of Energy (DE-AC26-99BC15202) for support of this work.

REFERENCES

- [1] S. C. Cowin. Bone poroelasticity. *J. Biomech.*, 37:217–238, 1999.
- [2] Y. P. Arramon and S. C. Cowin. Hydraulic stiffening of cancellous bone. *FORMA*, 12:209–221, 1997.
- [3] A. J. Beaudoin, W. M. Mihalko, and W. R. Krause. Finite element modelling of polymethylmethacrylate flow through cancellous bone. *J. Biomech.*, 24:127–136, 1991.
- [4] M. S. Thompson, G. Flivik, R. Juliusson, A. Odgaard, and L. Ryd. A comparison of structural and mechanical properties in cancellous bone from the femoral head and acetabulum. *J. Eng. Med., Proc. Instn. Mech. Engrs. Part H*, 218:425–429, 2004.
- [5] P. W. Hui, P. C. Leung, and A. Sher. Fluid conductance of cancellous bone graft as a predictor for graft-host interface healing. *J. Biomech.*, 29:123–132, 1996.
- [6] A. Syahrom, M.R.A. Kadir, J. Abdualh, and A. Öchsner. Permeability studies of artificial and natural cancellous bone structures. *Med. Eng. Phys.*, 2012.
- [7] J.C.M. Teo, K.M. Si-Hoe, J.E.L. Keh, and S.H. Teoh. Correlation of cancellous bone micro architectural parameters from microCT to CT number and bone mechanical properties. *Mater. Sci. Eng. C*, 27:333–339, 2007.
- [8] D. Ulrich, B. Van Rietbergen, A. Laib, and P. Rügsegger. The ability of three-dimensional structural indices to reflect mechanical aspects of trabecular bone. *Bone*, 25:55–60, 1999.
- [9] W. E. Kenyon, P. I. Day, C. Straley, and J. F. Willemsen. A three-part study of NMR longitudinal relaxation properties of water-saturated sandstones. *SPE Formation Evaluation*, 3:622–636, 1988.
- [10] P. W. J. Glover, I. I. Zadjali, and K. A. Frew. Permeability prediction from MICP and NMR data using an electrokinetic approach. *Geophysics*, 71:F49–F60, 2006.
- [11] S. S. Kohles, J. B. Roberts, M. L. Upton, C. G. Wilson, L. J. Bonassar, and A. L. Schlichting. Direct perfusion measurements of cancellous bone anisotropic permeability. *J. Biomech.*, 34:1197–1202, 2001.
- [12] S. S. Kohles and J. B. Roberts. Linear poroelastic cancellous bone anisotropy: Trabecular solid elastic and fluid transport properties. *J. Biomech. Eng.*, 124:521–526, 2002.
- [13] R. S. Ochia and R. P. Ching. Hydraulic resistance and permeability in human lumbar vertebral bodies. *J. Biomech. Eng.*, 124:533–537, 2002.
- [14] M. J. Grimm and J. L. Williams. Measurement of permeability in human calcaneal trabecular bone. *J. Biomech.*, 30:743–745, 1997.
- [15] J. A. Ochoa and B. M. Hillberry. Permeability of bovine cancellous bone. *Transactions of the Orthopaedic Research Society*, 17:162, 1992.
- [16] E. A. Nauman, K. E. Fong, and T. M. Keaveny. Dependence of intertrabecular permeability on flow direction and anatomic site. *Ann. Biomed. Eng.*, 27:517–524, 1999.
- [17] J. Uh and A.T. Watson. Determining spatial distributions of permeability. *Transport in Porous Media*, 86:385–414, 2011.
- [18] A. T. Watson, J. T. Hollenshead, J. Uh, and C. T. P. Chang. NMR determination of porous media property distributions. *Annual Reports on NMR Spectroscopy*, 48:113–144, 2002.
- [19] K. Seto, J. T. Hollenshead, A. T. Watson, C. T. P. Chang, and J. C. Slattery. Determination of permeability distributions using NMR velocity imaging. *Transport in Porous Media*, 42:351–388, 2001.
- [20] J. C. Slattery. *Momentum, Energy, and Mass Transfer in Continua*. Krieger, New York, NY, 1981.

- [21] S. Whitaker. Diffusion and dispersion in porous media. *AIChE J.*, 13:420–427, 1967.
- [22] J. C. Slattery. *Advanced Transport Phenomena*. Cambridge University Press, New York, 1998.
- [23] C. T. P. Chang and A. T. Watson. NMR imaging of flow velocity in porous media. *AIChE J.*, 45:437–444, 1999.
- [24] J. V. Beck and K. J. Arnold. *Parameter Estimation in Engineering and Science*. Wiley, New York, 1977.
- [25] P.-H. Yang and A. T. Watson. A Bayesian methodology for estimating relative permeability curves. *SPE Res. Eng.*, 6:259–265, 1991.
- [26] L. L. Schumaker. *Spline Functions: Basic Theory*. John Wiley and Sons, New York, NY, 1981.